The Astrophysical Journal, 668: L83–L86, 2007 October 10

NUMERICAL SIMULATIONS OF SLOW STANDING WAVES IN A CURVED SOLAR CORONAL LOOP

M. Selwa,[1] L. Ofman,[1] and K. Murawski[2]

Received 2007 June 26; accepted 2007 August 20; published 2007 September 27

ABSTRACT

We consider slow standing waves that are impulsively excited in a curved solar coronal loop. The numerical model we implement includes the effect of nonlinearity in the frame of two-dimensional ideal magnetohydrodynamics. We discuss the role of curved magnetic field lines and of the slow and fast pulses overlapping at one of the loop's footpoints in the excitation and attenuation of slow standing waves. We find that slow waves can be excited faster in curved loops than in slabs due to the combined effect of the pulse inside and outside the loop.

Subject headings: Sun: corona — Sun: oscillations

Online material: color figures

1. INTRODUCTION

Slow standing waves in hot coronal loops have been studied both observationally and theoretically. They were observed for the first time by Wang et al. (2002) using the SUMER instrument on *SOHO*. From the observations it was inferred that the slow standing waves are triggered at the loop's footpoints, and only the fundamental mode of the slow standing wave was observed. Some properties of these waves have been studied in detail by Wang et al. (2003a, 2003b, 2005). Numerical studies of slow standing waves aim to explain excitation and attenuation of the slow standing waves. For instance, Ofman & Wang (2002) showed that slow standing waves are strongly attenuated by thermal conduction. Nakariakov et al. (2004) and Tsiklauri et al. (2004) showed that only the second harmonic is excited, regardless of the spatial position of heat deposition. On the other hand, Selwa et al. (2005a) showed that pulses close to a footpoint excite the fundamental mode of the slow standing wave, while pulses close to the apex excite the second harmonic. In addition, these authors studied the influence of the pulse and loop parameters on the excitation and attenuation of slow standing waves. Mendoza-Briceño et al. (2004) discussed the effect of gravity on the attenuation of slow standing waves, while Taroyan et al. (2005) showed that the observed slow standing waves may have their origin in footpoints of the loop. Selwa et al. (2006) showed that footpoint excitation in a curved loop may lead to excitation of the fundamental slow standing mode, while excitation below the apex of the loop leads to the excitation of the first harmonic. Ogrodowczyk & Murawski (2007) found that slow waves are excited faster and attenuated more efficiently in a 2D straight slab than in a 1D loop due to coupling of slow waves with fast magnetosonic waves.

This Letter is organized as follows: The numerical model is described in § 2. The numerical results are presented in § 3. The Letter is concluded by a brief summary of the main results in § 4.

[1] Department of Physics, Catholic University of America, 620 Michigan Avenue, NE, 200 Hannan Hall, Washington, DC 20064; and NASA Goddard Space Flight Center, Code 671, Greenbelt, MD 20771; mselwa@helio.gsfc.nasa.gov, leon.ofman@gsfc.nasa.gov.

[2] Astrophysics and Gravity Theory Group, Institute of Physics, UMCS, ul. Radziszewskiego 10, 20-031 Lublin, Poland; kmur@kft.umcs.lublin.pl.

2. NUMERICAL MODEL

We describe the coronal plasma by the ideal MHD equations:

$$\frac{\partial \varrho}{\partial t} + \boldsymbol{\nabla}\cdot(\varrho \boldsymbol{V}) = 0, \tag{1}$$

$$\frac{\partial(\varrho \boldsymbol{V})}{\partial t} + \boldsymbol{\nabla}\cdot[(\varrho \boldsymbol{V})\boldsymbol{V}] = -\boldsymbol{\nabla} p + \frac{1}{\mu}(\boldsymbol{\nabla}\times \boldsymbol{B})\times \boldsymbol{B}, \tag{2}$$

$$\frac{\partial E}{\partial t} + \boldsymbol{\nabla}\cdot\left[\left(E + p + \frac{B^2}{2\mu}\right)\boldsymbol{V} - \frac{\boldsymbol{B}(\boldsymbol{B}\cdot\boldsymbol{V})}{\mu}\right] = 0, \tag{3}$$

$$\frac{\partial \boldsymbol{B}}{\partial t} = \boldsymbol{\nabla}\times(\boldsymbol{V}\times\boldsymbol{B}). \tag{4}$$

Here μ is the magnetic permeability, ϱ is the mass density, $\boldsymbol{V}$ is the flow velocity, p is the gas pressure, $\boldsymbol{B}$ is the divergence-free ($\boldsymbol{\nabla}\cdot\boldsymbol{B} = 0$) magnetic field, and plasma energy density is expressed as

$$E = \frac{\varrho V^2}{2} + \frac{p}{\gamma - 1} + \frac{B^2}{2\mu}\ , \tag{5}$$

where $\gamma = 5/3$ is the adiabatic index.

We adopt and modify the coronal arcade model that was described recently by Selwa et al. (2005b, 2006, 2007). In this model magnetic field components are given as

$$\boldsymbol{B}_e = B_0[\cos(x/\Lambda_B),\ 0,\ -\sin(x/\Lambda_B)]e^{-z/\Lambda_B}. \tag{6}$$

Here B_0 is the magnetic field at the reference level $z = 0$, and $\Lambda_B = 2L/\pi$ is the magnetic scale height, with L being the horizontal half-width of the arcade, chosen as $L = 100$ Mm.

Following Selwa et al. (2005b, 2006, 2007), a constant background mass density $\varrho_e = 10^{-12}$ kg m^{-3} is assumed in the entire spatial region. With such an assumption the Alfvén speed in the ambient medium becomes $V_{Ae} = V_{A0}e^{-z/\Lambda_B} = |B_e|/(\mu\varrho_e)^{1/2}$, where $V_{A0} = 1$ Mm s^{-1} is the Alfvén speed at $z = 0$. In this model V_{Ae} decays exponentially with height z but as $\Lambda_B = 200/\pi$ Mm, the decay rate is small. For a potential magnetic arcade the equilibrium pressure $p_e = \varrho_e c_{se}^2/\gamma$ has to be constant. Here $c_{se} = 0.35V_{A0}$ is the sound speed in the ambient medium.

We consider a loop embedded in the arcade in such a way

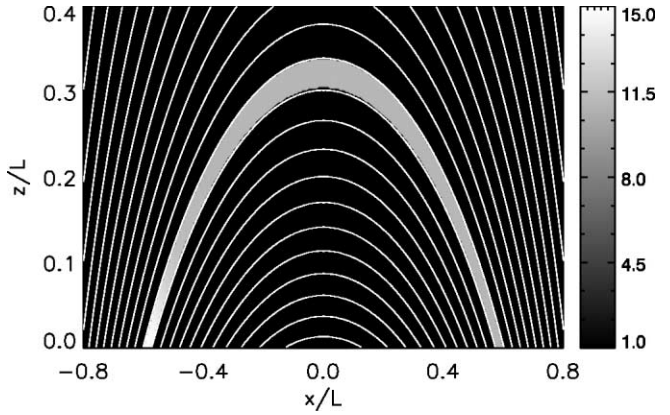

FIG. 1.—Initial configuration of the loop in a presence of the pulse that is launched in the left footpoint. Mass density contours (color scale in units of $\varrho_e = 10^{-12}$ kg m^{-3}) represent a loop denser than the corona. Magnetic field lines are shown as solid white lines. [*See the electronic edition of the Journal for a color version of this figure.*]

that its edges follow two specific magnetic field lines. We prescribe that the inner and outer field lines cross the base of the arcade at $|x| = L_f - 2a_f$ and $|x| = L_f$, respectively. Here $L_f = 0.6L$, $a_f = 0.0125L$. Such a loop does not have a perfect circular shape, but its length can be estimated as $l = 146$ Mm. The equilibrium structure of the loop is shown in Figure 1. The mass density is enhanced in the loop compared to the ambient medium. We choose the mass density contrast $d = \varrho_i/\varrho_e = 10$, where ϱ_i denotes the mass density within the loop and ϱ_e corresponds to the ambient medium. Note that both the Alfvén speed and the sound speed within the loop are smaller than in the ambient medium: $V_{Ai} = V_{Ae}/\sqrt{d}$, $c_{si} = c_{se}/\sqrt{d}$.

Perturbations in equations (1)–(4) can be excited in such a loop in numerous ways. As we are interested in excitation of the fundamental mode, we launch a hot pulse in gas pressure and mass density at the loop footpoint (Selwa et al. 2005a):

$$\delta f(x, z, t = 0) = \frac{A_f f_0}{\cosh\left[(x - L_f)/w\right] \cosh\left(z/w\right)}. \qquad (7)$$

Here $f = [\varrho, p]$, $w = 10$ Mm is the pulse width which acts both in the loop's footpoint and ambient corona, and the relative amplitudes of the pulse are $A_\varrho = A_p/10 = 0.5$, corresponding to a pulse that is 6.4 times hotter than the corona, which is close to observations (Wang et al. 2003a).

3. NUMERICAL RESULTS

Equations (1)–(4) are solved numerically with the 2D MHD code EMILY (Jones et al. 1997) in an Eulerian box with the x- and z-dimensions $(-L, L) \times (0, 1.2L)$. This box is covered by a uniform grid of 300 × 600 numerical cells. Grid convergence studies, which are based on grid refinement, were performed to show that the numerical results are not affected by spatial resolution. We apply open boundary conditions, with zero-gradient extrapolation of all plasma variables, at the right, left, and top sides of the simulation region, thus allowing a wave signal to leave freely the simulation region. At the bottom of the simulation region the line-tying ($\boldsymbol{V} = 0$) boundary conditions are set to model the interaction between the denser photosphere and the overlying plasma layers.

Figure 2 exhibits periodic density and flow fluctuations, obtained at the loop's apex. Following the method described by

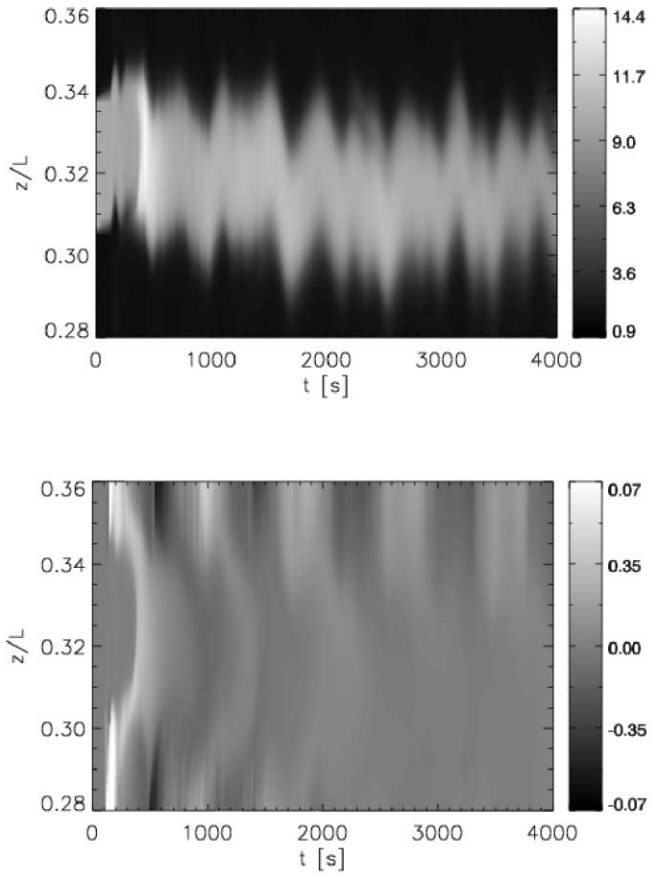

FIG. 2.—Time signatures of the mass density (*top*) and the x-component of velocity (*bottom*) in the neighborhood of the loop's apex. The density is measured in units of ϱ_e and velocity in units of V_{A0}. [*See the electronic edition of the Journal for a color version of this figure.*]

Selwa et al. (2005b), we extract the signal at the loop's apex (Fig. 3), determined as the position at which the mass density attains its maximum value. Note approximately a quarter–wave-period phase shift between the mass density and velocity (Fig. 3). By fitting a damped sine curve to the velocity and mass density profiles in the corresponding time signatures, we find a wave period $P = 835$ s.

In order to examine whether the standing mode is excited

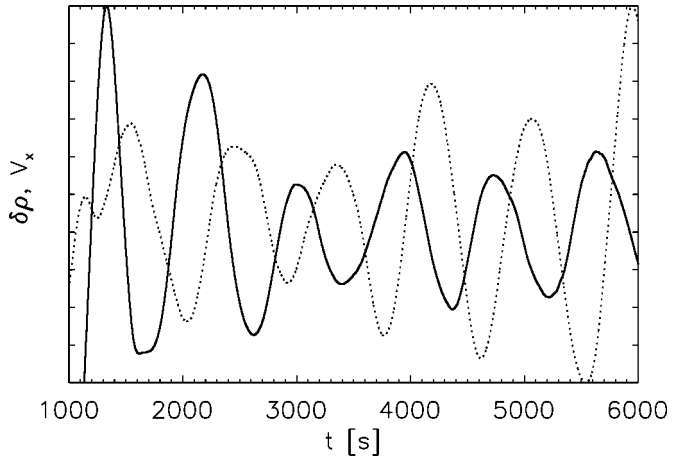

FIG. 3.—Time signatures of the mass density (*dotted line*) and the x-component of velocity (*solid line*) at the loop's apex.

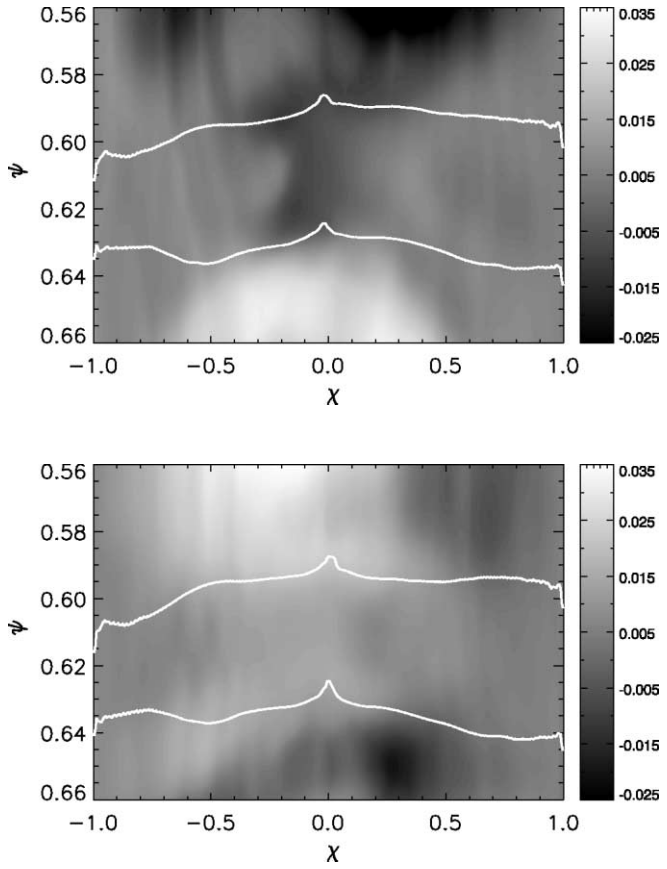

FIG. 4.—Spatial profiles of the parallel (to the loop) component of velocity for $t = 1575$ s (*top*) and $t = 2000$ s (*bottom*), plotted in flux coordinates. White lines indicate a position of the loop that at the equilibrium is straight in the flux coordinates. [*See the electronic edition of the Journal for a color version of this figure.*]

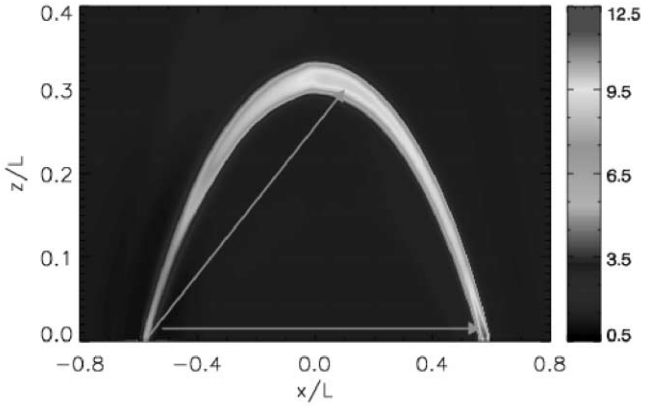

FIG. 5.—Spatial profile of the mass density (color scale, units of ϱ_e) for $t = 950$ s. Two mass density enhancements (patches inside the loop, marked with arrows) are observed in the loop. [*See the electronic edition of the Journal for a color version of this figure.*]

we plot the component of the velocity parallel to the loop axis (Fig. 4) in flux coordinates (Oliver et al. 1996). We find that spatial profiles exhibit behavior that is characteristic of the fundamental standing slow mode, similarly to the ones studied by Selwa et al. (2005a) in a 1D approximation.

To determine when the standing mode is generated we apply the excitation criterion (Selwa et al. 2005a). According to this criterion the standing wave is excited in the system if a phase shift between the mass density and velocity in the time signatures differs by no more than 20% from the quarter–wave period. As the time signatures show such a shift in the range 1500 s $< t <$ 4000 s, we find the excitation time $t_{\rm ex} = 1575$ s $= 1.6P$. In this case the standing wave is excited about a factor of 2 faster than in the straight loop (Selwa et al. 2005a). However, the results still differ from the observations (Wang et al. 2002, 2003a, 2003b), which show that the standing mode is excited within 1 wave period after a trigger takes place. From a fit of the damped sine function we find that the attenuation time is $\tau = 1202$ s $= 1.44P$. This value is smaller than the observational damping time for loops observed with SUMER (Wang et al. 2002, 2003a, 2003b).

4. SUMMARY AND DISCUSSION

A possible explanation of the reduction of the excitation time of slow standing waves in a curved structure in comparison to the straight loop is the different way the pulse acts on the loop, which in this case is independent of the shape of the pulse only if the pulse covers both the loop's footpoint and the surrounding corona. In the straight structure the pulse propagates along the loop and reflects from the photospheric layer. As a consequence, it takes several reflections of the pulse at the loops' footpoints to establish a standing wave in the loop. In a curved loop the pulse acts twofold: one part which is set inside the loop propagates along the loop, while another which comes from the part of the pulse outside the loop footpoint reaches the other footpoint while propagating through the ambient corona (patches marked with arrows in Fig. 5) as a fast magnetosonic wave. By comparing the speed with which the slow wave propagates inside the loop, $c_{si} = c_{se}/\sqrt{d} = 0.11V_{\rm Ae}$, to the Alfvén speed in the ambient corona, we see that the time in which the fast wave excited by the pulse in one of the footpoints propagates toward the opposite footpoint, $\delta t_f = 2L_f/V_{\rm Ae} =$ 120 s, is much smaller than the predicted time of propagation of slow wave inside the loop, $\delta t_s = 2l/c_{si} = 1327$ s. From this point of view we can approximate that the fast wave excited outside one of the footpoints of the loop reaches the opposite footpoint immediately, and in practice such an excitation mechanism produces a pulse at both footpoints nearly simultaneously, thus reducing the time needed to excite the slow standing wave. Evidently, this mechanism of excitation of standing slow waves can be efficient only in curved loops. According to Selwa et al. (2005a), excitation time decreases significantly with loop length. In our studies the loop was quite short compared to typical hot loops observed by SUMER. Based on a linear fit to the Selwa et al. (2005a) results for varying loop length (top panel of their Fig. 11), we can estimate the loop length for which the slow standing mode would be excited in less than 1 wave period in such a 2D curved geometry as $1.97l = 287$ Mm, which is in the range of typical hot coronal loop lengths observed by SUMER.

Note that the period of oscillations shown in Figures 2 and 3 coincides with the analytically predicted value $P = 2l/c_{se}$, where c_{se} is measured outside the loop. A possible explanation of that phenomenon comes from the fact that the standing wave inside the loop is generated as a consequence of the wave generated in ambient medium. Such a wave in the ambient corona draws along the wave inside the loop. If a pulse was propagating inside the loop with the sound speed $c_{se}/\sqrt{d}$, it should reach the apex at $t \sim 1300$ s; if it was propagating with c_{se}, it would reach the apex at $t \sim 200$ s. However, we observe

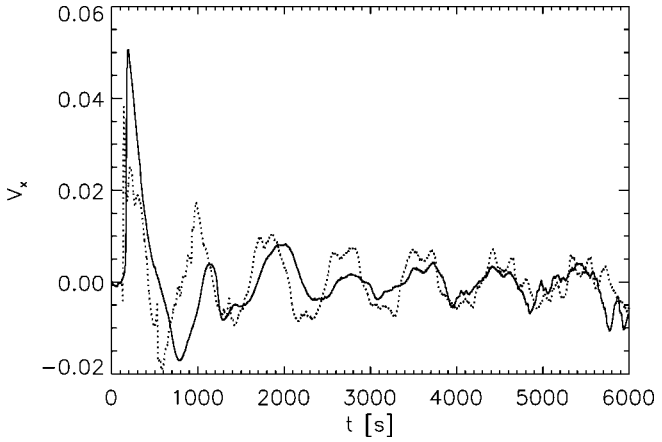

FIG. 6.—Time signatures of the x-component of velocity at the $x = 0$ line inside the loop ($z = 0.32L$; *solid line*) and at a small distance outside the loop ($z = 0.35L$; *dotted line*; normalized amplitude). The signal inside the loop is transferred at $t_s = 207.831$ s.

it at $t \sim 400$ s (with ~200 s delay to the propagation outside the loop). We look for the maximum correlation versus time lag t_s between signals inside and outside the loop (shown in Fig. 6). The correlation attains a maximum value of 0.72 for $t_s \simeq 208$ s.

As we work in a frame of ideal MHD, neither thermal conduction nor diffusion can play any role in the attenuation of slow standing waves. To understand better the attenuation mechanism, we solve the dispersion relation of the phase speed $V_{\rm ph}$ for the plasma inside (subscript i) and outside (subscript e) the loop:

$$V_{\rm ph}^4 - V_{\rm ph}^2 (c_{se(i)}^2 + V_{{\rm A}e(i)}^2) + c_{se(i)}^2 V_{{\rm A}e(i)}^2 \cos^2(\theta) = 0, \qquad (8)$$

where θ is the propagation angle. The phase speed components corresponding to the slow wave are shown in Figure 7. The phase speed of slow waves in the direction not parallel to the field is small, but greater than zero due to the finite value of β (Fig. 7) and increases outside the loop, so the wave which propagates with the maximum phase speed inside the loop

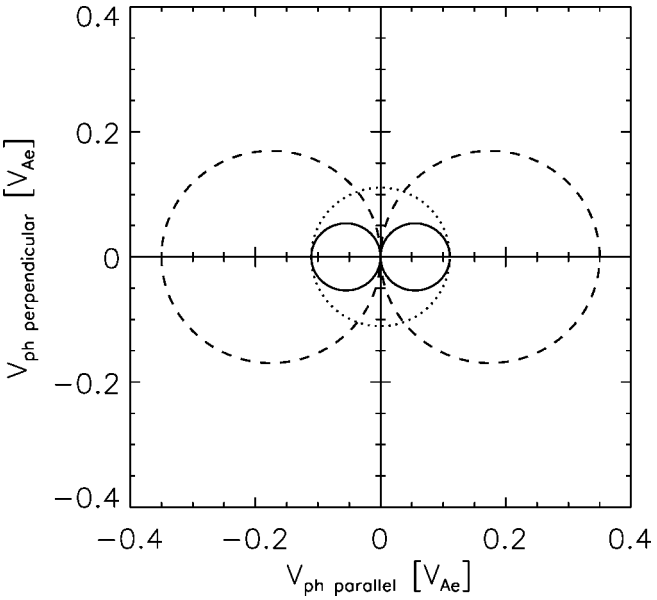

FIG. 7.—Polar diagram of phase speeds of slow magnetoacoustic waves inside (*solid line*) and outside (*dashed line*) the loop. The sound speed inside the loop, c_{si}, is marked with the dotted line.

(dotted circle in Fig. 7) can propagate obliquely and can be refracted out of the loop. The above dispersion relation is for a homogeneous medium. In our case the magnetic field is curved and since the slow wave that is parallel to the field at some point in the loop becomes oblique, as it propagates along the loop, leakage can take place due to wave refraction.

The work of M. S. and L. O. was financially supported by the NASA SEC Theory Program and NASA grant NNG06GI55G. The work of K. M. was supported by a grant from the State Committee for Scientific Research, Republic of Poland, with MNiI grant 2 PO3D. The magnetohydrodynamic code used in this study was developed by Ogden S. Jones, Uri Shumlak, Scott Eberhardt, and Bogdan Udrea, and provided through the sponsorship of the AFOSR program.

REFERENCES

Jones, O. S., Shumlak, U., & Eberhardt, D. S. 1997, J. Comput. Phys., 130, 231
Mendoza-Briceño, C. A., Erdélyi, R., & Sigalotti, L. Di G. 2004, ApJ, 605, 493
Nakariakov, V. M., Tsiklauri, D., Kelly, A., Arber, T. D., & Aschwanden, M. J. 2004, A&A, 414, L25
Ofman, L., & Wang, T. J. 2002, ApJ, 580, L85
Ogrodowczyk, R., & Murawski, K. 2007, A&A, 467, 311
Oliver, R., Hood, A. W., & Priest, E. R. 1996, ApJ, 461, 424
Selwa, M., Murawski, K., & Solanki, S. K. 2005a, A&A, 436, 701
Selwa, M., Murawski, K., Solanki, S. K., & Wang, T. J. 2007, A&A, 462, 1127
Selwa, M., Murawski, K., Solanki, S. K., Wang, T. J., & Tóth, G. 2005b, A&A, 440, 385
Selwa, M., Solanki, S. K., Murawski, K., Wang, T. J., & Shumlak, U. 2006, A&A, 454, 653
Taroyan, Y., Erdélyi, R., Doyle, J. G., & Bradshaw, S. J. 2005, A&A, 438, 713
Tsiklauri, D., Nakariakov, V. M., Arber, T. D., & Aschwanden, M. J. 2004, A&A, 422, 351
Wang, T. J., Solanki, S. K., Curdt, W., Innes, D. E., & Dammasch, I. E. 2002, ApJ, 574, L101
Wang, T. J., Solanki, S. K., Curdt, W., Innes, D. E., Dammasch, I. E., & Kliem, B. 2003a, A&A, 406, 1105
Wang, T. J., Solanki, S. K., Innes, D. E., & Curdt, W. 2005, A&A, 435, 753
Wang, T. J., Solanki, S. K., Innes, D. E., Curdt, W., & Marsch, E. 2003b, A&A, 402, L17